Journal of Magnetism and Magnetic Materials 465 (2018) 768–774

Contents lists available at ScienceDirect

Journal of Magnetism and Magnetic Materials

journal homepage: www.elsevier.com/locate/jmmm

Research articles

Cobalt spin states investigation of Ruddlesden-Popper $La_{2-x}Sr_xCoO_4$, using X-ray diffraction and infrared spectroscopy

T. Ghorbani-Moghadam[a], A. Kompany[a,b,*], M.M. Bagheri-Mohagheghi[c], M. Ebrahimizadeh Abrishami[b]

[a] Materials and Electroceramics Lab, Department of Physics, Ferdowsi University of Mashhad, Mashhad, Iran
[b] Nano Research Center, Ferdowsi University of Mashhad, Mashhad, Iran
[c] School of Physics, Damghan University, Damghan, Iran

ARTICLE INFO

Keywords:
Ruddlesden-Popper
Jahn-Teller distortion
Spin state
XRD
IR spectroscopy

ABSTRACT

Ruddlesden-Popper (RP) $La_{2-x}Sr_xCoO_4$ (x = 0.7, 0.9, 1.1, 1.3) were synthesized by a modified sol-gel route. The synthesized samples were characterized by XRD, FE-SEM technique, iodometric titration, FT-FIR spectroscopy and VSM analysis. The variation of Co-O bond length obtained from Rietveld refinements and the related peak shifts in the FT-FIR spectra showed that Co^{3+} has both LS and IS spin states. It is found that the population of Co^{3+} in the LS state decreases and IS state increases with increasing Sr concentration. Jahn-Teller effect was identified in the FT-FIR absorption bands, corresponding to the vibration modes of Co bonds with the apical and equatorial oxygen atoms. The ferromagnetic characteristic of $La_{0.7}Sr_{1.3}CoO_4$, obtained by VSM, revealed the increase of Co^{3+} IS population by Sr doping, in agreement with XRD and FT-FIR results. The shift and split of the IR absorption bands with the change in the structural parameters are proposed to be an applicable tool to probe the spin states and Jahn-Teller effect in $La_{2-x}Sr_xCoO_4$ compounds.

1. Introduction

Ruddlesden-Popper (RP) oxides with the general formula $A_{n+1}B_nO_{3n+1}$ are interesting materials, due to their promising applications in superconductors, magnetoresistors, dielectric and piezoelectric ceramics, catalysts for water splitting and regenerative fuel cells [1–7].

In $Ln_{2-x}A_xTMO_4$ compounds (Ln: lanthanides, A: alkaline-earth metal and TM: transition metal) by increasing the alkaline-earth content the charge neutrality is compensated by variation of TM oxidation states [8]. In addition, the spin and oxidation states of TMs affect the structural and transport properties of RP compounds [9–11]. In the perovskites with cobalt atoms at B sites, there are three spin states for Co^{3+} namely: the low spin (LS: $t_{2g}^6 e_g^0$), intermediate spin (IS: $t_{2g}^5 e_g^1$) and high spin (HS: $t_{2g}^4 e_g^2$) state [12]. The transition between the spin states depends on the crystal field splitting energy (Δ_{cf}) and the intra-atomic exchange energy (J_{ex}) of t_{2g} and e_g levels (Hund's coupling rule), which results in the electron distribution between t_{2g} and e_g levels [13]. Several factors, such as doping electrons or holes, temperature and external mechanical pressure can affect the correlation between Δ_{cf} and J_{ex}, resulting some phenomena such as Jahn-Teller distortion (JT) and spin blockade [14–17]. The spin state transitions of Co^{3+} ions in $La_{2-x}Sr_xCoO_4$ are still under investigation and there are different reports on Co electronic state configurations. For example a theoretical approach, based on the Hartree-Fock approximation, showed that Co^{3+} ions for $x < 0.5$ in $La_{2-x}Sr_xCoO_4$ are in the HS state, while in the samples with $0.5 \leq x < 1.1$ mixed spin states of the HS-LS were observed [18]. Chang et al. reported that Co^{3+} has shown to be in the LS state with insulating behavior related to the spin blockade phenomenon in $La_{0.5}Sr_{1.5}CoO_4$ [19]. According to Moritomo et al. Co^{3+} in $La_{2-x}Sr_xCoO_4$ exhibits a transition from HS to IS for $x > 0.8$ [20]. Tealdi et al. proposed that Co^{2+}, Co^{3+} and Co^{4+} are in HS, LS and LS states, respectively at room temperature [21].

Although, there are many reports on cobalt spin states in perovskites, the appearance of the IS state in RP type of cobalt oxides is still under debate and needs to be further studied. In this research, $La_{2-x}Sr_xCoO_4$ (x = 0.7, 0.9, 1.1, 1.3) single phase were successfully synthesized by a modified sol-gel method and XRD, FT-IR and FE-SEM techniques were performed. The observed magnetic hysteresis loops, by vibrating sample magnetometer (VSM) analysis at room temperature, supported our FT-IR and XRD results.

* Corresponding author at: Materials and Electroceramics Lab, Department of Physics, Ferdowsi University of Mashhad, Mashhad, Iran.
E-mail address: kompany@um.ac.ir (A. Kompany).

https://doi.org/10.1016/j.jmmm.2018.06.062
Received 25 February 2018; Received in revised form 11 June 2018; Accepted 21 June 2018
Available online 21 June 2018
0304-8853/

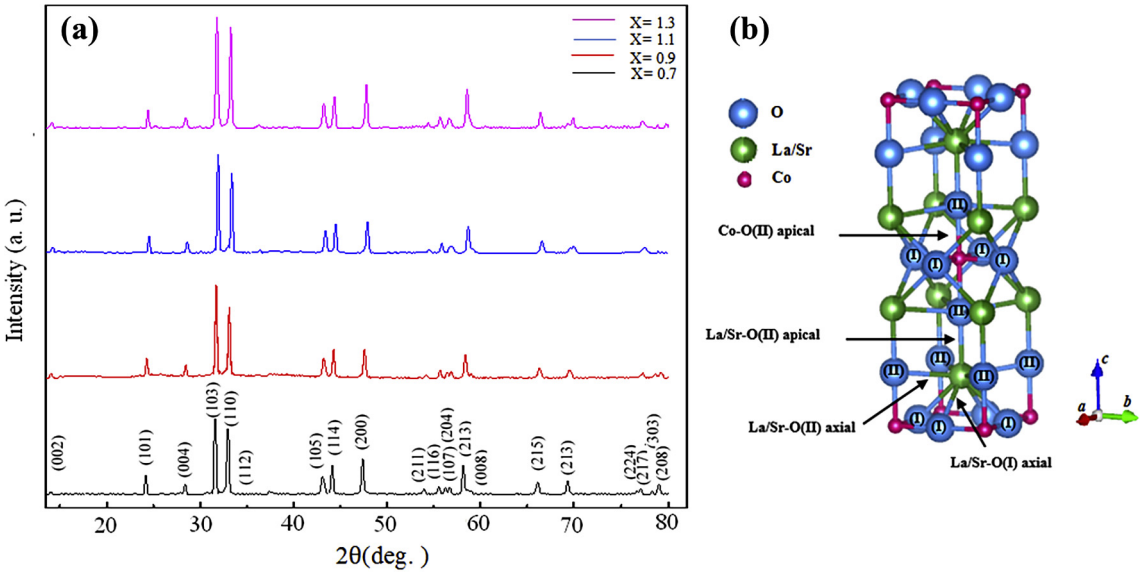

Fig. 1. (a) XRD patterns of $La_{2-x}Sr_xCoO_4$ (x = 0.7, 0.9, 1.1 and 1.3). The peaks are indexed for tetragonal I4/mmm space group and (b) the cation coordination of the apical and equatorial oxygen atoms in RP structure (n = 1).

Table 1
Sr content in $La_{0.7}Sr_{1.3}CoO_4$ sample, obtained from XRF and calculated from formula.

Element	%Weight	%Atomic (XRF)	%Atomic (formula)
Sr	38.541	40.035	42

2. Experimental procedures

2.1. Synthesis

$La_{2-x}Sr_xCoO_4$ (x = 0.7, 0.9, 1.1, 1.3) were synthesized through a modified sol-gel method. The starting materials were $La(NO_3)_3{\cdot}6H_2O$, $Sr(NO_3)_2$, $Co(NO_3)_2{\cdot}6H_2O$ and gelatin as the polymerization and stabilization agent. The nitrates were added gradually into deionized water, under stirring, at room temperature. Gelatin was dissolved separately in deionized water and stirred for 30 min at 60 °C. Then, the ionic solution was added to the aqueous solution of gelatin and subsequently kept at 80 °C-oil bath until a red color resin was obtained. The resin (gel) was heated at 220 °C for 2 h and the resulting black powder was then ground and calcined at 900 °C for 4 h.

2.2. Characterization methods

The structure of the calcined powders, with different Sr concentrations, were analyzed by X-ray diffraction (GNR, Explorer, CuKα, λ = 1.5406Å). The structural data were refined by Rietveld method with Full Prof (2.00) and the atomic model was built using the Vesta software package [22]. The particle size and morphology of the prepared samples were investigated using field emission scanning electron microscopy (FE-SEM: TE-SCAN, MIRA3). Infrared transmittance spectra were recorded at room temperature, by the standard Perkin-Elmer Spectrum 400MIR/FIR spectrometer, in the region 200–700 cm^{-1}. The magnetic characterization of the prepared samples was performed, through VSM measurements at room temperature.

3. Results and discussion

3.1. Structural analysis

Fig. 1(a) shows the X-ray diffraction patterns of the synthesized $La_{2-x}Sr_xCoO_4$ (x = 0.7, 0.9, 1.1, 1.3) powders at room temperature. These patterns indicate that the crystal structure of all samples is tetragonal with the space group I4/mmm. Fig. 1(b) represents the K_2NiF_4-type structure of $La_{2-x}Sr_xCoO_4$. As shown in this figure, there are two types of oxygen atoms, O(4c) and O(4e) located in *ab* planes and *c* direction, respectively. So, there are two types of Co-O bonds with different lengths: the axial Co-O(I) corresponding to equatorial bonds in perovskite layers and the apical Co-O(II) bond along the *c* direction. XRF measurements were used to obtain the weight percent and the atomic weight percent of Sr content in $La_{0.7}Sr_{1.3}CoO_4$ which are given in Table1. The actual atomic weight is very close to the formula value. The FE-SEM images of $La_{2-x}Sr_xCoO_4$ samples are given in Fig. 2. The particle size distribution was obtained by counting 100 particles from three different batches. The corresponding histograms in Fig. 2 show that the average particle size value is almost the same in all samples and below 100 nm. The unit cell parameters, the Co-O and (La/Sr)-O bond lengths and (La/Sr)-O-Co angles, obtained from Rietveld refinements, are presented in Table2. Substitution of Sr atoms at La sites affects the unit cell parameters which results in the variation of Co-O and (La/Sr)-O bond lengths and also the bond angles.

The cobalt valence values as a function of Sr concentration, determined from iodometric titration are given in Table2. Our results showed that the increase of Sr concentrations has led to the increase of cobalt valence from 2.68 for X_{sr} = 0.7 to 3.21 for X_{sr} = 1.3. As can be seen in Table 1, the lattice parameter *a* and the unit cell volume decrease with the increase of Co valance, while the *c* parameter first decreases for x < 1 and then increases for x > 1. Since the ionic radius of Sr^{2+} (1.30 Å) is larger than that of La^{3+} (1.216 Å), increasing the volume of the unit cell by doping Sr in $La_{2-x}Sr_xCoO_4$ is logically

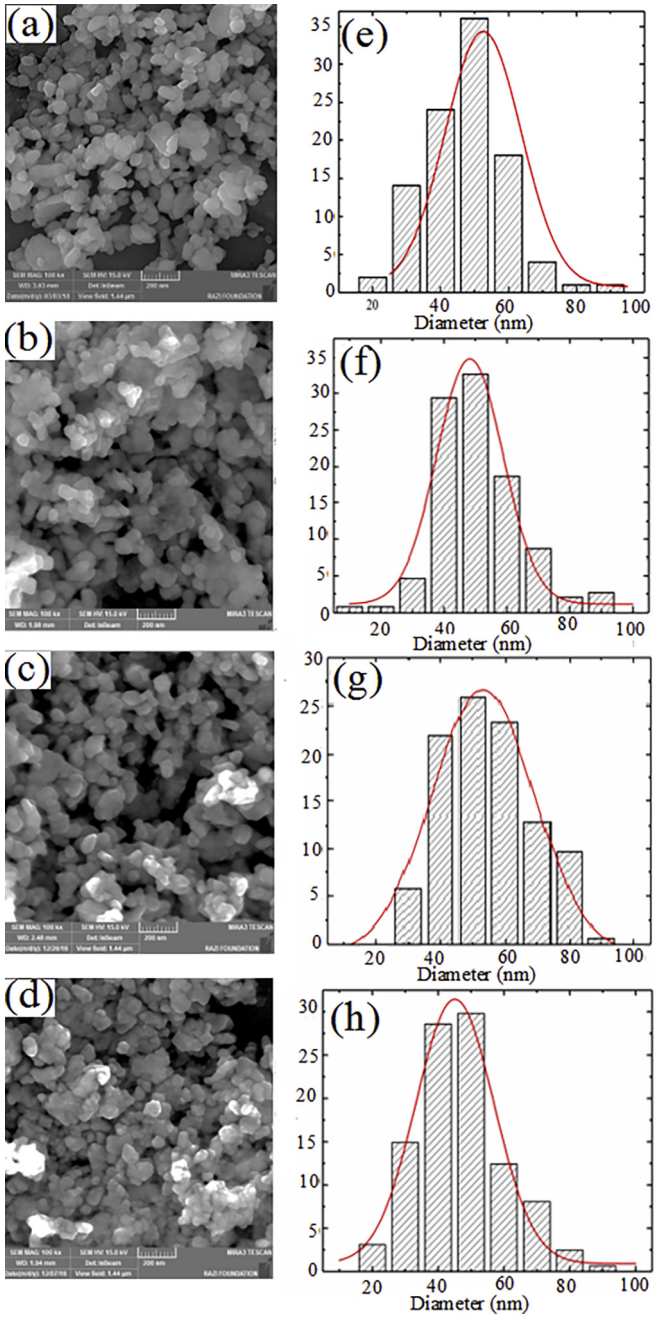

Fig. 2. (a) FE-SEM images, and (b) the particle size distribution histograms of the synthesized $La_{0.7}Sr_{1.3}CoO_4$.

expected. However, the decrease of the volume cell is not merely related to the ionic radii difference of La and Sr. In fact, substitution of La by Sr causes the change of Co valence to higher values (Co^{2+} to Co^{3+} and Co^{3+} to Co^{4+}), which results in the decrease of Co ionic radius that seems to be more effective regarding the lattice constants variation, compared to the ionic radius difference of La and Sr. Fig. 3 shows the changes of Co-O(I) and Co-O(II) bond lengths, calculated by Rietveld refinement versus the cobalt valency obtained from iodometric titration. As shown in this Fig., the Co-O(I) bond length decreases with the increase of the Co valance, as a consequence of Co oxidation and spin state variation. However, the Co-O(II) bond length in the sample with $X_{Sr} = 1.1$ (Co valance = 3.06) has increased, which can be related to JT effect due to the increase of Co^{3+} IS population [21].

3.2. FT-FIR characterization

The characteristic of IR transmittance spectra of the calcined samples, in the range of 200–700 cm^{-1}, are presented in Fig. 4. The wavenumbers related to the vibration modes of the IR bands are summarized in Table 3. As shown in Fig. 4, by increasing Sr concentration the IR spectra for $X_{Sr} = 1.3$ is more smooth in the wavenumber range of $250\ cm^{-1} \le k \le 350\ cm^{-1}$ compared to the others, due to the screening effect. For A_2BO_4 structures, there are seven infrared-active modes ($3A_{2u} + 4E_u$) [23]. The E_u and A_{2u} vibration modes are related to the in-plane oxygen and the apical oxygen connected bonds, respectively. The E_u vibration modes, in the ranges of $616\ cm^{-1} \le k \le 672\ cm^{-1}$ and $397\ cm^{-1} \le k \le 421\ cm^{-1}$, are attributed to the stretching vibration and deformation modes of Co-O(I) bonds, respectively. The vibration modes in the ranges of $460 \le k \le 512\ cm^{-1}$, $250 \le k \le 400\ cm^{-1}$ and $150 \le k \le 250\ cm^{-1}$ correspond to the (La/Sr)-O(II)-Co and (La/Sr)-O(II) stretching and the lattice modes, respectively [23–25].

3.2.1. Co-O(I) vibration modes

As mentioned earlier, the spin states of Co^{2+} and Co^{4+} in $La_{2-x}Sr_xCoO_4$ are believed to be HS and LS respectively at room temperature [21]. In the FT-FIR spectrum of layered perovskite $La_{1.3}Sr_{0.7}CoO_4$ (Fig. 4), the absorption band of Co-O(I) stretching mode at around 616 cm^{-1} is due to the hybridization of Co^{2+} (HS)-3d and Co^{3+} (IS)-3d with O-2p. In addition, Co^{3+} (LS)-O which is more covalent than both Co^{2+} (HS)-O and Co^{3+} (IS)-O [26] results in a vibration mode at about 672 cm^{-1}. By increasing the Sr content to 0.9, the vibration mode at lower energies increases from 616 cm^{-1} ($X_{Sr} = 0.7$) to 634 cm^{-1} ($X_{Sr} = 0.9$). This can be attributed to the decrease of Co^{2+} HS state population and increasing the Co^{3+} IS state which is more covalent than Co^{2+} HS. These variations of IR vibration modes have been reported for Co^{3+} transitions between IS and LS in cobalt-contained perovskites [27–29].

By increasing Sr content from 0.9 to 1.1 and 1.3, the wavenumber decrease of Co-O(I) stretching vibration modes from 670 cm^{-1} to about 640 cm^{-1} occurs as a result of Co^{3+} IS state stabilization. In the samples with $X_{sr} = 1.1$ and 1.3, a shoulder around 630 cm^{-1} which is observed in Fig. 4 is due to JT distortion originating from the presence of both Co^{3+} IS and Co^{4+} LS. This shoulder is more pronounced in $La_{0.7}Sr_{1.3}CoO_4$, since Co^{3+} IS state is more stable comparing to Co^{3+} LS. The slight increase in the stretching energies of Co-O(I) in $La_{0.7}Sr_{1.3}CoO_4$, in comparison with $La_{0.9}Sr_{1.1}CoO_4$, can be related to the increase of Co^{4+} LS population [21]. Another absorption peak at 421 cm^{-1} and a shoulder at about 400 cm^{-1}, observed in the FT-FIR spectrum of $La_{1.3}Sr_{0.7}CoO_4$ (Fig. 4), correspond to Co-O(I) deformation mode. The presence of this shoulder is attributed to JT distortion of Co^{2+} HS. The characteristic peak shift toward lower energies (from 421 cm^{-1} to 397 cm^{-1}) with increasing Sr doping from 0.7 to 1.3 is another evidence of the population decrease of Co^{3+} LS state and the same time increase of IS state.

3.2.2. (La,Sr)-O(II)-Co vibration modes

The absorption band around 450–500 cm^{-1} (Fig. 4) is related to the stretching-shrinking mode of (La,Sr)-O(II)-Co, involving the apical oxygen bond. In the FT-FIR spectrum of $La_{1.3}Sr_{0.7}CoO_4$ (Fig. 4), there is an absorption peak at 486 cm^{-1} and a shoulder at about 510 cm^{-1}

Table 2
The unit cell parameters, atomic bond lengths and cation coordination from Rietveld refinements data and the obtained Co valence from iodometric titration of the synthesized $La_{2-x}Sr_xCoO_4$ (x = 0.7, 0.9, 1.1, 1.3).

	$La_{1.3}Sr_{0.7}CoO_4$	$La_{1.1}Sr_{0.9}CoO_4$	$La_{0.9}Sr_{1.1}CoO_4$	$La_{0.7}Sr_{1.3}CoO_4$
a(Å)	3.825	3.813	3.803	3.803
c(Å)	12.509	12.488	12.510	12.526
Volume (Å^3)	183.065	181.563	180.997	181.210
Density (g/cm^3)	6.619	6.486	6.318	6.123
Co-O(I) (Å)	1.912	1.906	1.901	1.9017
Co-O(II) (Å)	2.141	2.005	2.05	2.020
La/Sr-O(II) (axial) (Å)	2.734	2.712	2.707	2.702
La/Sr-O(II) (apical) (Å)	2.374	2.526	2.46	2.488
La/Sr-O(I) (Å)	2.585	2.562	2.578	2.587
La/Sr-O(II)-Co angle (degree)	81.560	83.790	83.4	84.38
$(La/Sr)_Z$	0.360	0.362	0.360	0.359
$(O(II))_Z$	0.171	0.160	0.164	0.161
Co valence (iodometric titration)	2.68	2.87	3.06	3.21

Wyckoff positions of tetragonal structure with the space group I4/mmm (No. 139): Co at 2a (0, 0, 0), O(I) at 4c (0, 0.5, 0), O(II) and La/Sr at 4e (0, 0, z).

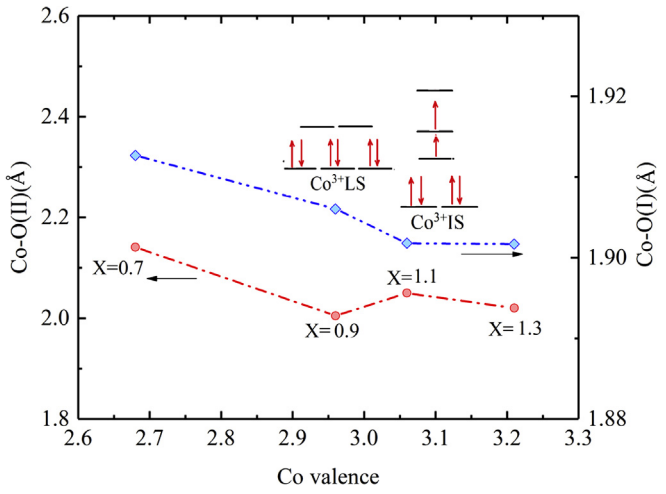

Fig. 3. Co-O(I) and Co-O(II) bond lengths obtained from Rietveld refinement calculations vs. Co valence in $La_{2-x}Sr_xCoO_4$ (x = 0.7, 0.9, 1.1, 1.3) compounds.

which confirm the JT distortion corresponded to Co^{2+} HS and Co^{3+} IS, respectively. The considerable shift of the absorption peak from 486 cm^{-1} to about 512 cm^{-1}, recorded for the sample with X_{Sr} = 0.9, approves the substitution of Co^{2+} HS by Co^{3+} LS and IS [21]. However, by increasing Sr content from X_{Sr} = 1.1 to 1.3 there is a remarkable peak shift from 509 cm^{-1} to 468 cm^{-1} as well as the absorption band peak splitting which suggest the weakening of Co-O(II) due to a JT elongation of CoO_6 octahedral. This IR splitting, related to the JT elongation, is shown schematically in Fig. 3 [30,31].

3.2.3. (La, Sr)-O(II) vibration modes

Fig. 5 shows the trend of the absorption band positions corresponding to (La/Sr)-O(II) (axial and apical) versus (La/Sr)-O(II) bond lengths and (La/Sr)-O(II)(axial)-Co angles, obtained from Rietveld refinement. The change of (La/Sr)-O(II)(axial) bond lengths shows that the stretching and deformation vibration energies increase with the decrease of the bond lengths, Fig. 5(a). Although Co^{3+} spin state transition was not observed in (La/Sr)-O(II)(axial), the trend of (La/Sr)-O(II)(apical) in Fig. 5(b) indirectly confirms the stabilization of Co^{3+} LS in $La_{1.1}Sr_{0.9}CoO_4$ and Co^{3+} LS transition to IS in $La_{0.9}Sr_{1.1}CoO_4$. Since the Co-O(II)(apical)-La angle is 180°, the strong Co^{3+} LS-O(II) bond in $La_{1.1}$ $Sr_{0.9}CoO_4$, comparing to Co^{2+} HS-O(II) in $La_{1.3}Sr_{0.7}CoO_4$, results in higher stretching and deformation energies in $(La/Sr)\text{-}O(II)_{apical}$, despite the increase of the bond lengths. In fact, the change in $(La/Sr)\text{-}O(II)_{apical}$ bond length is a clear evidence for Co^{3+} LS stabilization. By increasing the Sr content from 0.9 to 1.1, the increase observed in the vibration energies originates from the decrease of La/Sr-O(II) bond length. As shown in Fig. 5(c), Co^{3+} LS stabilization causes a similar trend in (La/Sr)-O(II)(axial)-Co angle. We propose that the $(La/Sr)\text{-}O(II)_{axial}$-Co angle can be another indicator for investigating the distortion of the La environment and the octahedral distortion.

4. Magnetization measurement

The variation of the magnetization (M) versus applied magnetic field (H) of $La_{2-x}Sr_xCoO_4$ samples, at room temperature, are given in Fig. 6. The magnetic hysteresis loops show the weak ferromagnetic behavior of the prepared samples. The magnetization loop is not saturated up to a magnetic field of 1000Oe which is characteristic of the antiferromagnetic ordering of the spins [32]. The existence of small hysteresis in the M-H curves indicates that Co^{3+} are in both LS and IS states. The increase of Co^{3+} IS state population, by doping Sr, results in the appearance of ferromagnetic behavior in $La_{0.7}Sr_{1.3}CoO_4$. This result is due to the double exchange interaction between Co^{2+} HS-Co^{3+} IS and Co^{3+} IS-Co^{4+} LS [33], supporting the stabilization of Co^{3+} IS for Xsr = 1.3 deduced from XRD and FT-IR analyses.

5. Conclusion

$La_{2-x}Sr_xCoO_4$ (x = 0.7, 0.9, 1.1, 1.3) were synthesized by a modified sol-gel method. The synthesized samples were characterized by XRD spectroscopy, FE-SEM technique, iodometric titration, FT-FIR and VSM analyses. The structural properties obtained from Rietveld refinements revealed that the bond length of Co-O(I) and Co-O(II) decreases with the increase of Co valance. This is due to the reduction of the ionic radius of Co, as a result of the oxidation states increase and the change in Co spin states. Furthermore, Co^{3+} is in both LS and IS spin states in all samples. However, by increasing Sr dopant from X_{Sr} = 0.7 to 1.3 the population of Co^{3+} LS state decreased and Co^{3+} IS state increased. FT-FIR spectra of the synthesized samples showed the

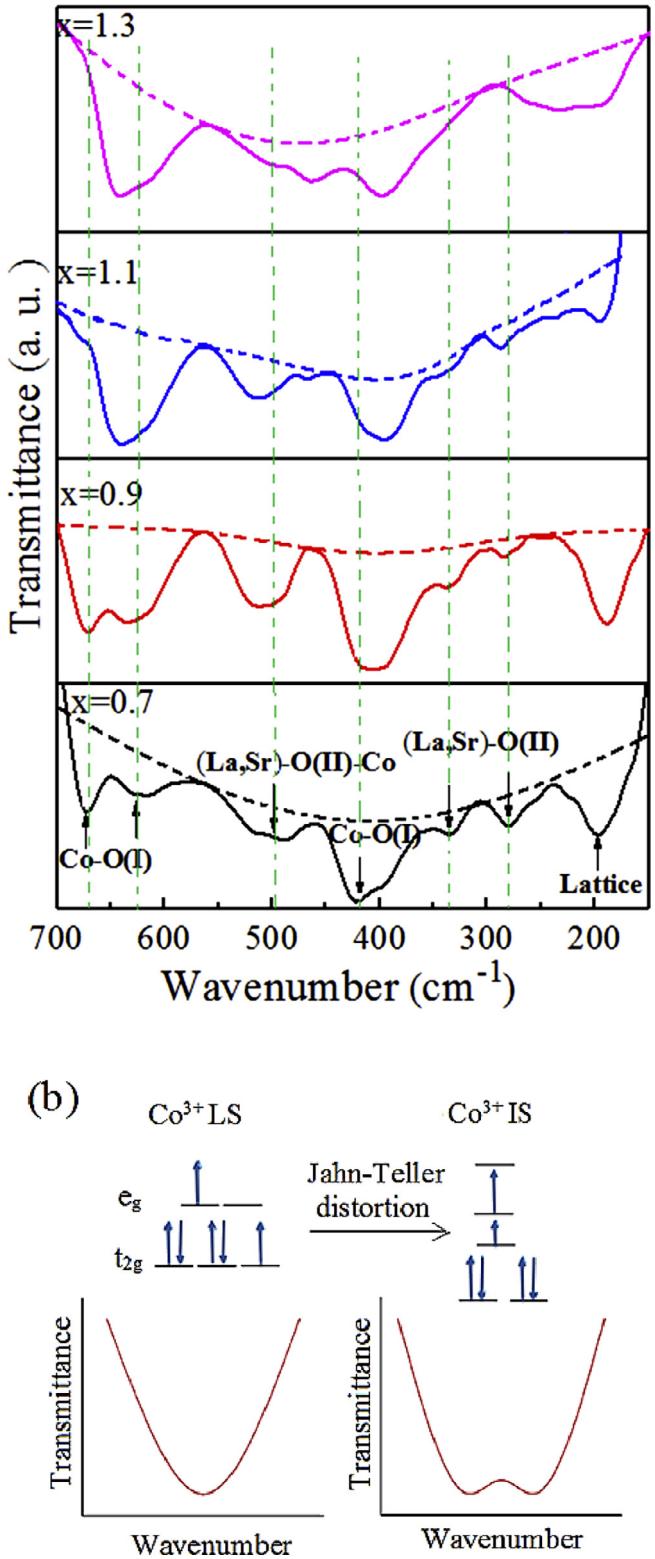

Fig. 4. (a) FT-FIR spectra of $La_{2-x}Sr_xCoO_4$ (x = 0.7, 0.9, 1.1, 1.3) and (b) the hypothetical transmittance spectrum corresponding to 3d-energy levels of Co^{3+} LS and splitting of the transmittance spectrum, related to 3d-energy levels of Co^{3+} IS due to the Jahn-Teller elongation. The baselines are shown by dashed lines.

characteristic of the vibration modes, corresponding to Co-O(I), (La/Sr)-O(II)-Co and La/Sr-O(II) bonds. The absorption bands, related to Co-O(I) and Co-O(II) vibration modes, exhibited two significant phenomena:(i) The increase of Co^{3+} IS state population resulted in the

Table 3
The wavenumber (cm^{-1}) and the assignment of the FT-FIR bands of the synthesized $La_{2-x}Sr_xCoO_4$.

symmetry	$La_{1.3}Sr_{0.7}CoO_4$	$La_{1.1}Sr_{0.9}CoO_4$	$La_{0.9}Sr_{1.1}CoO_4$	$La_{0.7}Sr_{1.3}CoO_4$	assignment
E_u	672, 616	670, 634	641	643	Co-O(I)-Co stretching
A_{2u}	486	512	509	468	La/Sr-O(II)-Co stretching
E_u	421	406	397	397	Co-O(I)-Co deformation
A_{2u}	336	338	340	–	Deformation of La/Sr-O(II)
E_u	280	284	286	–	Stretching of La/Sr-O(II)
A_{2u}	–	248	236	234	Lattice distortion
E_u	196	188	194	200	Lattice distortion

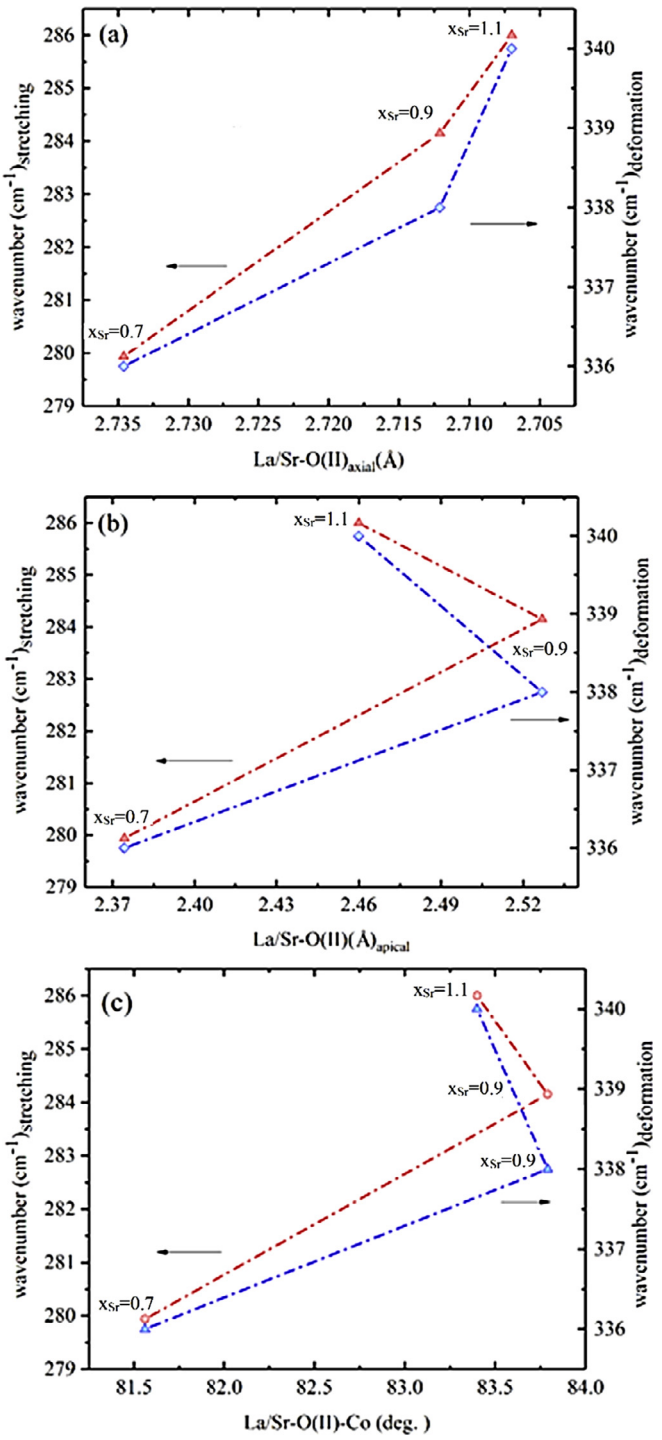

Fig. 5. The variations of the stretching and deformation vibration modes, corresponding to La/Sr-O(II), versus (a) $(La/Sr)\text{-}O(II)_{axial}$, (b) $(La/Sr)\text{-}O(II)_{apical}$ bond lengths and (c) $(La/Sr)\text{-}O(II)_{axia}$l-Co angle, obtained from Rietveld refinement.

vibration modes shifts and (ii) Jahn-Teller effect deduced from splitting of the bands. Also, the octahedral distortion was investigated using the trends of the La/Sr-O(II) bond lengths and (La/Sr)-O(II)(axial)-Co angles and the shifts observed in their corresponding IR absorption bands. The existence of hysteresis in the magnetization curves of $L_{2-x}Sr_xCoO_4$ supported the presence of Co^{3+} in both LS and IS states, obtained by XRD and FT-IR data analyses. The ferromagnetic behavior of $La_{0.7}Sr_{1.3}CoO_4$ indicated that Co^{3+} in IS state in this compound is more stable than in the other prepared samples.

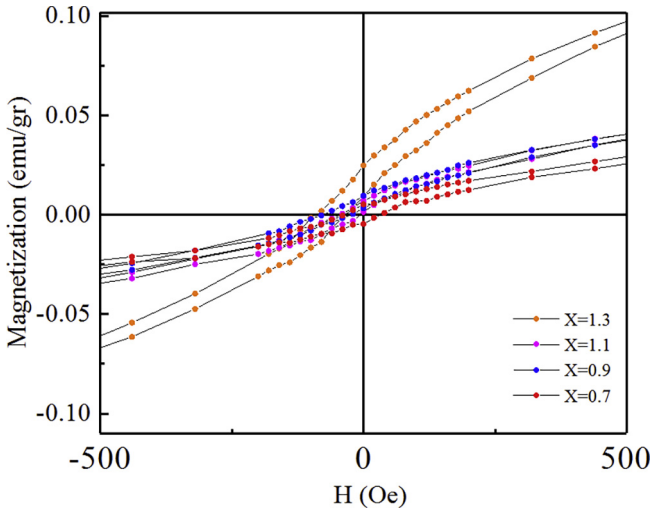

Fig. 6. The magnetic hysteresis loop of $La_{2-x}Sr_xCoO_4$ (x = 0.7, 0.9, 1.1, 1.3) at room temperature.

Acknowledgement

This work has been supported by the Vice President for Research and Technology, Ferdowsi University of Mashhad, under code number: 3.40687.

References

[1] J. Goodenough, Electronic and ionic transport properties and other physical aspects of perovskites, Rep. Prog. Phys. 67 (11) (2004) 1915.
[2] T. Takeguchi, T. Yamanaka, H. Takahashi, H. Watanabe, T. Kuroki, H. Nakanishi, Y. Orikasa, Y. Uchimoto, H. Takano, N. Ohguri, Layered perovskite oxide: a reversible air electrode for oxygen evolution/reduction in rechargeable metal-air batteries, J. Am. Chem. Soc. 135 (30) (2013) 11125–11130.
[3] V. Kharton, A. Viskup, A. Kovalevsky, E. Naumovich, F. Marques, Ionic transport in oxygen hyperstoichiometric phases with K_2NiF_4-type structure, Solid State Ionics 143 (3) (2001) 337–353.
[4] T. Matsuura, J. Tabuchi, J. Mizusaki, S. Yamauchi, K. Fueki, Structure, electrical conductivity, and Seebeck coefficient of single crystals x = 0.0, 0.5, 1.0 and 1.5, J. Phys. Chem. Solids 49 (12) (1988) 1403–1408.
[5] M. Ebrahimizadeh Abrishami, M. Risch, J. Scholz, V. Roddatis, N. Osterthun, C. Jooss, Oxygen evolution at manganite perovskite Ruddlesden-Popper type particles: trends of activity on structure, Valence and Covalence, Materials 9 (11) (2016) 921–940.
[6] A. Kompany, T. Ghorbani-Moghadam, S. Kafash, M.E. Abrishami, Frequency dependence of Néel temperature in $CaMnO_{3-\delta}$ ceramics: synthesized by two different methods, J. Magn. Magn. Mater. 349 (2014) 135–139.
[7] M. Zhou, T. Bak, J. Nowotny, M. Rekas, C. Sorrell, E. Vance, Defect chemistry and semiconducting properties of calcium titanate, J. Mate. Sci. Mater. Electron. 13 (12) (2002) 697–704.
[8] V. Vashook, H. Ullmann, O. Olshevskaya, V. Kulik, V. Lukashevich, L. Kokhanovskij, Composition and electrical conductivity of some cobaltates of the type $La_{2-x}Sr_xCoO_{4.5-x/2\pm\delta}$, Solid State Ionics 138 (1) (2000) 99–104.
[9] C. Tealdi, L. Malavasi, F. Gozzo, C. Ritter, M.C. Mozzati, G. Chiodelli, G. Flor, Correlation between transport properties and lattice effects in the $NdCoO_3$ based catalysts and sensor materials, Chem. Mate. 19 (19) (2007) 4741–4750.
[10] P.G. Radaelli, S.-W. Cheong, Structural phenomena associated with the spin-state transition in $LaCoO_3$, Phys. Rev. B 66 (9) (2002) 094408.
[11] C. Frontera, J.L. García-Muñoz, A.E. Carrillo, M.A. Aranda, I. Margiolaki, A. Caneiro, Spin state of Co^{3+} and magnetic transitions in R $BaCo_2O_{5.50}$ (R = Pr, Gd): Dependence on rare-earth size, Phys. Rev. B 74 (5) (2006) 054406.
[12] S. Sugano, Multiplets of Transition-Metal Ions in Crystals, Academic Press, New York, 1970.
[13] G. Maris, Y. Ren, V. Volotchaev, C. Zobel, T. Lorenz, T. Palstra, Evidence for orbital ordering in $LaCoO_3$, Phys. Rev. B 67 (22) (2003) 224423.
[14] D. Fuchs, C. Pinta, T. Schwarz, P. Schweiss, P. Nagel, S. Schuppler, R. Schneider, M. Merz, G. Roth, H.V. Löhneysen, Ferromagnetic order in epitaxially strained $LaCoO_3$ thin films, Phys. Rev. B 75 (14) (2007) 144402.
[15] D. Fuchs, P. Schweiss, P. Adelmann, T. Schwarz, R. Schneider, Ferromagnetic order in the electron-doped system $La_{1-x}Ce_xCoO_3$, Phys. Rev. B 72 (1) (2005) 014466.
[16] J.-S. Zhou, J.-Q. Yan, J. Goodenough, Bulk modulus anomaly in R CoO_3 (R = La, Pr, and Nd), Phys. Rev. B 71 (22) (2005) 220103.
[17] T. Vogt, J. Hriljac, N. Hyatt, P. Woodward, Pressure-induced intermediate-to-low spin state transition in $LaCoO_3$, Phys. Rev. B 67 (14) (2003) 140401.
[18] J. Wang, Y. Tao, W. Zhang, D. Xing, Theoretical study on the spin-state transition in

doped $La_{2x}Sr_xCoO_4$, J. Phys. Condens. Matter 12 (33) (2000) 7425.
[19] C.-F. Chang, Z. Hu, H. Wu, T. Burnus, N. Hollmann, M. Benomar, T. Lorenz, A. Tanaka, H.-J. Lin, H. Hsieh, Spin blockade, orbital occupation, and charge ordering in La $_{1.5}$ Sr $_{0.5}$ CoO $_4$, Phys. Rev. Lett. 102 (11) (2009) 11640.
[20] Y. Moritomo, K. Higashi, K. Matsuda, A. Nakamura, Spin-state transition in layered perovskite cobalt oxides: La_{2-x} Sr_x CoO_4 ($0.4 \leq x \leq 1.0$), Phys. Rev. B 55 (22) (1997) R14725.
[21] C. Tealdi, C. Ferrara, L. Malavasi, P. Mustarelli, C. Ritter, G. Chiodelli, Y.A. Diaz-Fernandez, High-temperature neutron diffraction study of La_{2-x} Sr_x CoO_4: Correlation between structure and transport properties, Phys. Rev. B 82 (17) (2010) 174118–174126.
[22] K. Momma, F. Izumi, VESTA: a three-dimensional visualization system for electronic and structural analysis, J. Appl. Crystallogr. 41 (3) (2008) 653–658.
[23] A.E. Lavat, E.J. Baran, IR-spectroscopic behaviour of AA′ BO_4 oxides belonging to the K_2 NiF_4 structural type, J. Alloys Compd. 368 (1) (2004) 130–134.
[24] L. Chen, C. Lu, Y. Lu, Z. Fang, Y. Ni, Z. Xu, Microwave absorption and infrared performance of $Sm_{0.5}$ $Sr_{0.5}$ Co_{1-x} Ni_xO 3 ($0 \leq x \leq 1.0$) with the $_K2Ni_F4$ structure, RSC Adv. 3 (12) (2013) 3967–3972.
[25] M. Daturi, G. Busca, E. Magnone, M. Ferretti, FT-IR skeletal study of RBa_2 $Cu_{3O7-}y$ (R = Ln or Y) and $N_{d2-}x$ Ce x Cu_O 4 cuprate powders, J. Solid State Chem. 119 (1) (1995) 36–44.
[26] T. Saitoh, T. Mizokawa, A. Fujimori, M. Abbate, Y. Takeda, M. Takano, Electronic structure and temperature-induced paramagnetism in $LaCoO_3$, Phys. Rev. B 55 (7) (1997) 4257.
[27] X. Che, L. Li, W. Hu, G. Li, Impact of hole doping on spin transition in perovskite-type cobalt oxides, Dalton Trans. 45 (26) (2016) 10539–10545.
[28] S. Zhou, L. Shi, J. Zhao, L. He, H. Yang, S. Zhang, Ferromagnetism in $LaCoO_3$ nanoparticles, Phys. Rev. B 76 (17) (2007) 172407.
[29] R. Mortimer, J. Powell, N. Vasanthacharya, Perturbation of the infrared spectrum of lanthanum cobaltate induced by vibronic coupling, Synth. Met. 71 (1) (1995) 2045–2046.
[30] M.D. Joesten, M.S. Hussain, P.G. Lenhert, Structure studies of pyrophosphate chelate rings. I. Crystal structures of tris-octamethylpyrophosphoramide complexes of cobalt (II), magnesium (II), and copper (II) perchlorates, Inorg. Chem. 9 (1) (1970) 151–161.
[31] P.T. Miller, P.G. Lenhert, M.D. Joesten, Crystal and molecular structure of tris (octamethyl methylene diphosphonic diamide) copper (II) perchlorate, Inorg. Chem. 11 (9) (1972) 2221–2227.
[32] E. Abdel-Khalek, H.M. Mohamed, Synthesis, structural and magnetic properties of La_{1-x} Ca_x FeO_3 prepared by the co-precipitation method, Hyperfine Interact. 222 (1) (2013) 57–67.
[33] H. Chang, Y. Gao, Q. Wu, X. Dong, Y. Li, Y. Pang, Influence of global and local distortion on magnetic properties of cubic $La_{06}Ba_{04-x}Ca_xCoO_3$, J. Magn. Magn. Mater. 396 (2015) 242–246.